Sensors & Transducers, Vol. 264, Issue 1, February 2024, pp. 19-25

www.sensorsportal.com

Sensors & Transducers

Published by IFSA Publishing, S. L., 2024
http://www.sensorsportal.com

A MEMS Based Large Travel Range Linear Actuator with a Good Minimum Step Size to Be Used in Mirror Shape Correction Applications

Ehsan Atash ZABAN and Dr Mehmet KUSAF
Department of Electrical and Electronic Engineering,
Cyprus International University, 99258, Nicosia, Northern Cyprus, Mersin 10, Turkey
Tel: 00989375437106
E-mails: 22009479@student.ciu.edu.tr, mkusaf@ciu.edu.tr

Received: 16 September 2023 /Accepted: 28 December 2024 /Published: 28 February 2024

Abstract: In this paper, a high-precision thermal linear micro actuator (*LMA*) with a large travel range is analyzed, simulated and presented. Physical functions can be performed by MEMS thanks to micro-actuators. The operation of various types of micro-actuators in many applications has been successful. There are two perspectives to categorize micro-actuators; one focused on driving forces and the other on mechanisms. Electric, magnetic, and flow fields can be utilized to generate force in the space between stationary and moving parts. The intrinsic actuation capabilities of materials like piezoelectric, magnetostrictive, and photo stretched materials also can be used in them. Changes in shape or volume caused by thermal expansion and phase transformations; such as the shape-memory effect and bubble formation are another important ways to reach a deformation in these types of actuators. In our proposed *LMA*, electro-thermal technique has been selected. The main components of the electro-thermal *LMA* proposed are substrate, slider, stopper, and forks. The slider is a long rectangle beam placed on a rail so that can move bidirectional, either up-ward or down-ward. A complex interesting technique, by using the stoppers and forks, results bidirectional movement of the slider. The stopper consists of arrayed electro-thermal chevrons (*EC*) and springy clutch. By applying a DC voltage of 1.5 V to the Red fork's ECs arrays, the minimum step size approximately 20 μm is achieved. Repeating steps sequentially generate a travel range of about 2 mm. For all simulations, the ANSYS software has been used. The *LMA* has the ability to displace heavy loads linearly and accurately. Minimum step size and large travel range of the *LMA* proposed make it useful to be used for Mirror Shape Correction application.

Keywords: MEMS, Mirror shape correction, Linear micro actuator (*LMA*), Electro-thermal chevrons (*EC*), The slider, The stopper, The forks, The springy clutch.

1. Introduction

Numerous researchers have studied *LMAs* and micro-deflections extensively for the purpose of arranging individual elements connected to the slider's head in micro electromechanical systems (MEMS). By repeating small deflections [1, 2], it is possible to move a slider linearly on a rail using certain techniques. Electrostatic, magneto-electric, piezoelectric, and electro-thermal techniques are the most effective ways to generate these deflections. It's unfortunate that micro scale applications tend to generate electrostatic and magneto-static forces that are too small. The devices can be operated in a resonant mode or applied a high voltage to achieve a

large travel range and overcome this issue. The Piezoelectric and Electro-thermal *LMAs* have the ability to create significant propulsion forces and deformation. Commercial MEMS foundries typically don't support piezoelectric materials during their fabrication processes. Electro-thermal LMAs [4] were the reason why we were drawn to them. Low power consumption and a large and linear travel range can be achieved using electro-thermal actuators as a promising solution. The IC voltage is the standard for standardizing the operating voltage of these actuators, unlike electrostatic-driven actuators. It is now easier to design them with no strict dimensional tolerances. Sliders in electro-thermal linear actuators allow for precise movement forward or backwards. Microsystem devices can generate linear movement through a variety of techniques. To move sliders, the initial method involves transferring momentum through a series of impacts beginning with number [1, 5, 16, 17]. The second method involves employing impact heads and notches the edges of the sliders, which significantly improves grip for sliders with a thickness of 6 to 8 mm. In the third method, the gripping occurs due to the frictional contact between the impact heads and the slider [9, 10] and leads to a beneficial resolution. The focus of this paper is on a sophisticated electro-thermal LMA that can travel up to 2 mm, and has a minimum step size of 20 mm and a travel range of 2 mm. An LMA for mirror shape correction application has been reported by [11, 19], but it does not have favorable power consumption or travel range. [12] has been reported a bulky LMA. Compared to [12], the proposed actuator is lighter and can be utilized in various important applications. In the following sections, several issues related to the LMA are discussed. The actuator mechanism and stopper are examined in Sections 2 and 3 with care, accuracy, and theoretical reasoning. The design of the slider is presented in Section 4. Section 5 is the conclusion.

2. Mechanism

Blue and green forks, along with the slider, stopper, and substrate, are all main components in this LMA. The schematic of the LMA can be seen in Fig. 1. Several EC arrays are used to move the slider in two directions and also release the springy clutches from the side wall. Two supports at an angle, known as 'anchors', secure the long beams that make up the ECs. Current passing through the beams from one terminal to another is what causes them to expand due to Joule heating. A deflection occurs in the y-direction of mathematical axis due to thermal expansion; consider Red ECs as an example. Deflecting the EC is affected significantly by both the length and angle of the beams. A smaller angle causes a greater deflection, while a larger angle causes a smaller deflection [7, 13, 20, 25]. The substrate acts as a chassis, and the slider is a solid long rectangular beam that can be moved on the substrate. Totally, two forks are available, one blue and one green. As depicted in Fig. 1, the stoppers are located on the four locations of the fork surface. The stopper's composition consists of the springy clutch and the ECs. To prevent the slider from shaking and moving randomly, the clutches are used. Besides, the stopper's ECs aid in generating the required force to connect the clutches to the substrate side walls. All clutches must be touched to the side walls of the slider during normal mode to prevent it from moving or shaking.

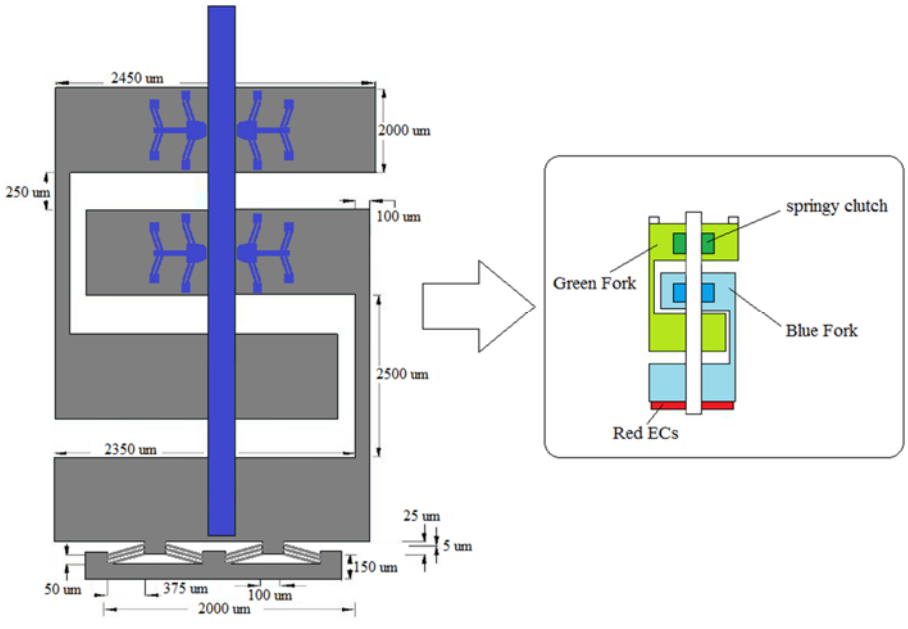

Fig. 1. The schematic of the *LMA* proposed.

Fig. 2 (a) shows that the slider is currently in rest mode, indicating that the entire fork's Green and Blue ECs are ON or activated. ON is the term for passing electrical current through electro-thermal cells and expanding polysilicon cells utilizing Joule's law. To start the operation, the Green fork's ECs are ON and the Blue fork's ECs are OFF, as shown in Fig. 2 (b). Upward or downward movement is achieved by applying electrical signals to all EC electrodes in a regular and sequential manner. The Blue fork moves forward and the slider dribbles in an interesting way when the voltages of the Green-Red and Blue forks are turned on and off, respectively. It is important to note that all the clutches are the same as in Fig. 2(c) in the previous step. Fig. 2(d) shows that the voltages applied to the ECs of the Green and Blue forks will be ON. As the temperature rises and cools the ECs, the Red fork's EC voltage drops to zero, causing the slider to contract smoothly. Refer to Fig. 2(e). This contraction leads to the Blue fork deflecting downward and the slider moving down-trend, shown in Fig. 2(e). A significant travel range could be achieved by repeating the sequences. To achieve upward movement, all steps can be reversed. In Fig. 3, you can see the schematic for the springy clutch. To obtain high precision and a large travel range, all parameters must be calculated carefully and separately [19, 9, 23, 24]. In short, generating a prototype of a complicated linear actuator necessitates the precise calculation, analysis of all dimensions, geometries, and material properties. Take into account which the generated friction force, appropriately, is enough to ensure the slider latching and stabilizing is successful during operation. To keep the sliders steady, the clutches can be fitted into the notches of LMAs. In these structures, despite the favorable force generated, resolution is limited. The expected resolution for these types of LMAs is approximately 100 nm. The LMA suggested reposition the slider with a force that could reach 8 mN either forward or backward.

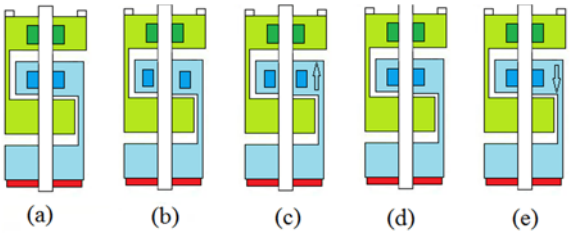

Fig. 2. Operation sequences (a) normal mode, (b) the Green fork´s *ECs* are *ON* and the Blue fork´s *ECs* are *OFF*, (c) The Green-Red and Blue fork´s *ECs* voltages applied are *ON*; *OFF*, (d) the slider is getting ready to contract, (e) downward deflection of Red fork's *Ecs*.

3. Analysis of the Stopper

By analyzing an inclined beam at the center of the chevrons shuttle, the springy clutch can be designed. Taking into account node A and assume that the shuttle is solid, as depicted in Fig. 4. When designing a springy clutch, it's crucial to take important parameters into account. Node A is deflected by the force generated F electro thermally in the central shuttle in the y-direction, which is equivalent to [14].

$$\begin{aligned} U^F \equiv U^A_{y\,total} &= U^A_{y1} + U^A_{y2} = \\ = F\frac{1}{2\left(\sin\theta_S \frac{EA_S{}^2}{l_s} + \cos\theta_S \frac{12EI_S{}^2}{l_s{}^3}\right)} &+ \\ +F\frac{1}{2\left(\sin\theta_c \frac{EA_c{}^2}{l_c} + \cos\theta_c \frac{12EI_c{}^2}{l_c{}^3}\right)} &= \\ = \frac{Fl_s}{EA_s}\frac{1}{2\left(\sin\theta_S{}^2 + \frac{\cos\theta_S{}^2}{\gamma_s}\right)} &+ \\ + \frac{Fl_c}{EA_c}\frac{1}{2\left(\sin\theta_c{}^2 + \frac{\cos\theta_c{}^2}{\gamma_c}\right)} & \end{aligned} \quad (1)$$

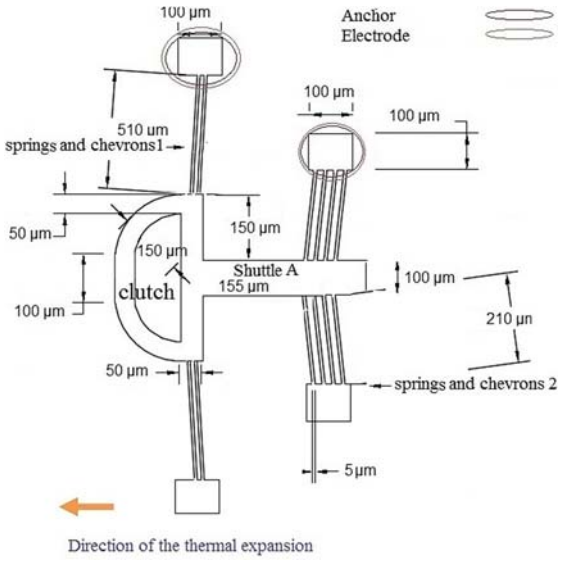

Fig. 3. The schematic of the springy clutch.

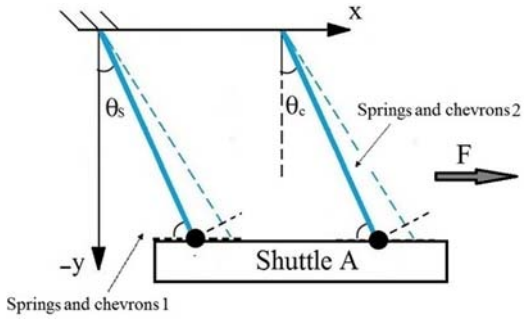

Fig. 4. A beam inclined joined at the central of chevrons´ shuttle.

The expression identified by 's' and 'c' is linked to chevrons 1 and 2, as indicated in Fig. 4. E is the Young's modulus of the material, while ls and lc are

the beam length. Ac represents the beam cross section and Is and Ic represents the moment of inertia of the cross section with respect to the out of plane axis z. As it said already, F is the electro-thermal force generated. Fig. 5 demonstrates the deflection of the springy clutch compared to the force applied. The reaction force in the x-direction is:

$$\begin{gathered} R_x^F \equiv R_x^A = \\ = cos\,\theta_s\, sin\,\theta_s \left(\frac{EA_s}{l_s} - \frac{12EI_s}{l_s^3}\right) U_{y1}^A + \\ + cos\,\theta_c\, sin\,\theta_c \left(\frac{EA_c}{l_c} - \frac{12EI_c}{l_c^3}\right) U_{y2}^A = \\ = F\frac{sin\,\theta_S cos\,\theta_S(\gamma_S - 1)}{2(\gamma_S\, sin\,\theta_S{}^2 + cos\,\theta_S{}^2)} + \\ + F\frac{sin\,\theta_c cos\,\theta_c(\gamma_c - 1)}{2(\gamma_c\, sin\,\theta_c{}^2 + cos\,\theta_c{}^2)}, \end{gathered} \tag{2}$$

and

$$\gamma_S = \frac{A_S l_S}{12 I_S}, \gamma_C = \frac{A_C l_C}{12 I_C} \tag{3}$$

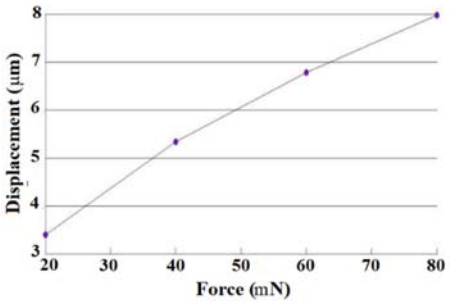

Fig. 5. Deflection of the springy clutch vs. the force applied.

The *SSFF* (static surface friction force) generated by the clutch's head is the same as:

$$F_{friction} = \mu_{static} F_u, \tag{4}$$

where Fu is the elastic potential force of the beam. Equations (1-3) can be taken into account in a primitive way to calculate the SSFF. The force generated by the chevrons1 and the chevrons2 causes the springy clutch to move toward the slider side wall. The electro-thermal mechanism and output heat conduction are responsible to actuate the chevrons. Following equations can be used theoretically to explain related operation.

$$Q_{output} = -Kw_s h_s \left(\frac{\partial T_s}{\partial x}\right)_{x+dx} \tag{5}$$

where K, w_s, h_s, T and x represents the thermal conductivity of poly-silicon, thickness, the height of the beams, temperature, and the fluctuating length of the beams, respectively. Equation (1) is substituted by equation (2), which means heat passing through thin beams. By neglecting the heat loss of the convection and radiation to the ambient, heat conduction is as following [15]:

$$Q_{input} = -Kw_s h_s \left(\frac{\partial T}{\partial x}\right)_x \tag{6}$$

By passing electrical current through the beams of the springy clutch:

$$Q_{j_s} = j_s^2 \rho w_s h_s dx, \tag{7}$$

$$\rho = \rho_0[1 + \zeta(T_s - T_o)], \tag{8}$$

$$J_s = \frac{V}{2\rho l_s}, \tag{9}$$

$$V = 2 l_s E_F, \tag{10}$$

where J_s, ρ, T_o, ζ and V represents current density, resistivity; substrate temperature, the temperature´s coefficient, *DC* voltage, respectively. T_o should be considered 293K. Figs. 6 and 7 display the springy clutch's deflection in relation to the *DC* voltage applied and the release time, respectively. Fig. 8(a-d) shows Model meshed, the clutch deformation, electrical voltage and current contours, respectively.

$$Q_{input} + Q_{J_s} = Q_{output} \tag{11}$$

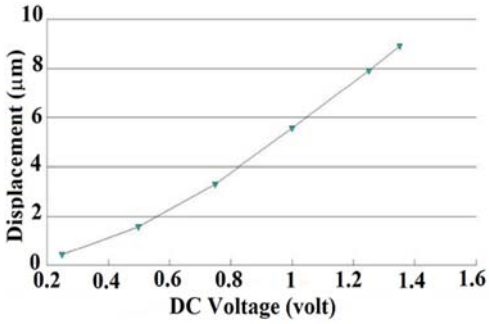

Fig. 6. Deflection of the clutch vs. the *DC* voltage applied.

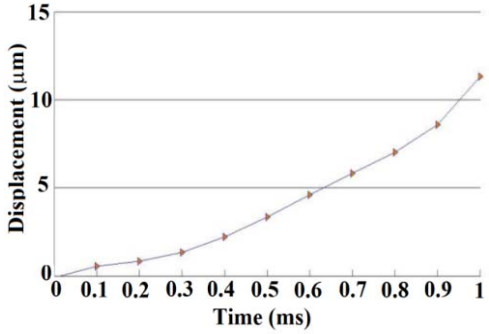

Fig. 7. The deflection of the clutch vs. the time.

The following equation can be formulated by substituting Equations (5) and (7) into Equation (11) and by limiting dx to 0.

$$K_p w_s h_s \left(\frac{\partial_2 T_s}{\partial x^2}\right) + j_s^2 \rho w_s h_s = 0 \tag{12}$$

The conductive cross-sectional area of the springy clutch is identical, so:

$$\frac{\partial {T_s}^2}{\partial x^2} = \frac{-j_s^2 \rho}{K}, \quad (13)$$

$$T(0) = T(l_s) = T_o, \quad (14)$$

$$T_s(x) = \frac{\rho J_S^S}{2K}(2l_s x - x^2) + T_O, \quad (15)$$

$$\Delta T_s = \int_0^{2l_s} \frac{T(x)_s - T_0}{2l_s} dx = \frac{V^2}{3K\rho} = \frac{P_r l_s}{3KA_s} \quad (16)$$

$$\Delta T_{s_{max}} = T_{s_{max}} - T_0 = \frac{V^2}{2K\rho} = = 1.5\Delta T_s, \quad (17)$$

$$P_r = I_r V \quad (18)$$

where P_r, I_r are electrical power and electrical current, respectively. Fig. 8(e) shows temperature´s distribution of the springy clutch. The average temperature of the springy clutch increases to ΔT_s, and ΔT_c, so deflection at node A in the y-direction is equal to [14]. By considering ΔT_s and ΔT_c, there is a compressive force $F_{\Delta T}$ in the hot arms [21]:

$$\begin{gathered} U^{\Delta T} \equiv U^A_{y_{total}} = \\ = \alpha \Delta T_s l_s \frac{\sin\theta_s}{\left(\sin\theta_S{}^2 + \cos\theta s \frac{12I}{A_s l_s^2}\right)} + \\ + \alpha \Delta T_c l_c \frac{\sin\theta_c}{\left(\sin\theta_c{}^2 + \cos\theta c \frac{12I}{A_c l_c^2}\right)} = \\ = \alpha \Delta T_s l_s \frac{\sin\theta_s}{\left(\sin\theta_S{}^2 + \frac{\cos\theta s^2}{\gamma_s}\right)} + \\ + \alpha \Delta T_c l_c \frac{\sin\theta_c}{\left(\sin\theta_c{}^2 + \frac{\cos\theta c^2}{\gamma_c}\right)}, \end{gathered} \quad (19)$$

where α is the coefficient of the thermal expansion. The contour plots of clutch deflection are shown in Fig. 8(a) when applying a *DC* voltage of 1.35 volt. The meshed model of the springy clutch by using couple field elements in *ANSYS* software is shown in 8(b). The reaction force generated in the x-direction is
equal to:

$$\begin{gathered} R_x^{\Delta T} \equiv R^A_{x_{total}} = \\ = -\alpha \Delta T_s E A_s \frac{\cos\theta_s}{\left(\sin\theta_s{}^2 \frac{Al_s^2}{12I_s} + \cos\theta_s{}^2\right)} - \\ - - \alpha \Delta T_c E A_c \frac{\cos\theta_c}{\left(\sin\theta_c{}^2 \frac{Al_c^2}{12I_c} + \cos\theta_c{}^2\right)} = \\ = -\alpha \Delta T_s E A_s \frac{\cos\theta_s}{(\sin\theta_s{}^2 \Psi_s + \cos\theta_s{}^2)} - \\ - - \alpha \Delta T_c E A_c \frac{\cos\theta_c}{(\sin\theta_c{}^2 \Psi_c + \cos\theta_c{}^2)} \end{gathered} \quad (20)$$

When considering the clutch release time, the total deflection is:

$$U^{\Delta T+F} = \left(U^{\Delta T} + U_s^F\right) + \left(U_c^{\Delta T} + U_c^F\right) \quad (21)$$

Total stiffness is:

$$U^{\Delta T+F} = \frac{(2\alpha \Delta T_s E A_s \sin\theta_s + F) + (2\alpha \Delta T_s E A_s \sin\theta_s + F)}{K_{tb}}, \quad (22)$$

$$\begin{gathered} K_{tb} \equiv \frac{F}{U_s^F} + \frac{F}{U_c^F} = \frac{2\left(\sin\theta_s{}^2 + \frac{\cos\theta_s{}^2}{\gamma_s}\right) E A_s}{l_s} + \\ + \frac{2\left(\sin\theta_c{}^2 + \frac{\cos\theta_c{}^2}{\gamma_c}\right) E A_c}{l_c} \end{gathered} \quad (23)$$

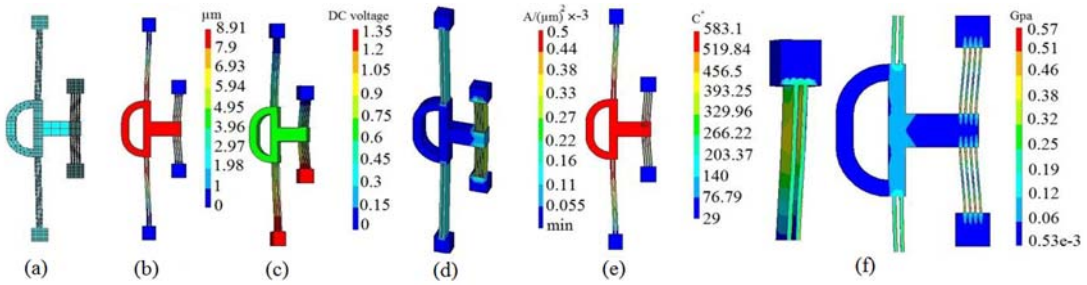

Fig. 8. Model meshed (a), the clutch deformation (b), the DC voltage (c), electrical current (d), temperature distribution (e), Stress counter of the clutch (f).

The expressions above can be approximated to the following:

$$K_{TA} = 2 \times mK_{tb} + 2\left(\sin\theta_c{}^2 + \frac{\cos\theta_c{}^2}{\gamma_c}\right) E A_c l_c^{-1}, \quad (24)$$

$$F_{\Delta T} \cong \frac{\alpha \Delta T_s}{\sin\theta_s{}^2} \frac{12EI_s}{L_{1s}^2} + \frac{\alpha \Delta T_c}{\sin\theta_c{}^2} \frac{12EI_c}{L_{1c}^2} \quad (25)$$

$$L_{1s} = 0.5\alpha \frac{L_s}{\cos\theta_s}, L_{1c} = 0.5\alpha \frac{L_c}{\cos\theta_c}, m = 2 \quad (26)$$

By compressing the springy clutch, approximately 5 m, a force of 40 mN can be generated. The two clutches have a total SSFF of 80 mN, by assuming the SSFC is roughly 0.2 [22]. Equation (4) allows the

slider to generate propulsion upward or downward force about 16 mN which guarantee the sider stability during operation. In other words, if the slider's propulsion forces exceed the total clutch's friction force, the grip would be faulted. A force of 80 mN can be achieved by applying a DC voltage of 1.25 volt. Fig. 8(f) illustrates the stress contours of the clutch that are less than 0.57 GPA due to the applied voltage which causes a deflection of approximately 7.9 µm.

4. Analysis of the Blue fork´s *ECs*

Equations of Section 3 are used to design the ECs of the Red fork. The couple field elements of ANSYS software are used to mesh the model and the electro-thermal analysis to be carried out. Table 1 shows the material properties of poly-silicon. The slider has a stroke of 2 µm when using a voltage of 1.5 V, as shown in Fig. 9.

Table 1. The Polysilicon properties used in the simulation.

Para	Value	Unit
Dens	2.33	$pg.\mu m^{-2}$
Ex	169	$pg.\mu m^{-1}ns^{-2}$
Prxy	0.28	–
Th ex	$2.6e^{-6}$	$°C^{-1}$
Res	e^{9}	$\mu m.\Omega$
Thermal conductivity	$14.9e^{-5}$	$pg.\mu m.ns^{-3}°C^{-1}$

The slider's deflection in relation to the force applied and time is shown in Figs. 10, 11. The temperature of the entire machine considers 293 K. Applying the appropriate voltage can result a minimum step size of 20 µm. The sequences can be repeated to achieve a large travel range, as demonstrated in Fig. 2. The contours of the deflection, stress, and temperature distribution in the Blue fork are shown in Fig. 12 (a-c), respectively. It should be noted that the stopper can be separated from the Blue fork's body in terms of electrical and thermal issues. The neighborhood of the stopper and the Blue fork electrical circuits can lead to an error. The SIO_2 could be utilized to separate boundaries.

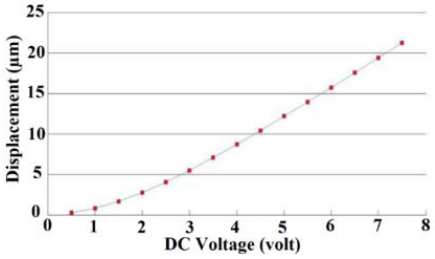

Fig. 9. Deflection of the *LMA´s* red fork vs. the *DC* voltage applied.

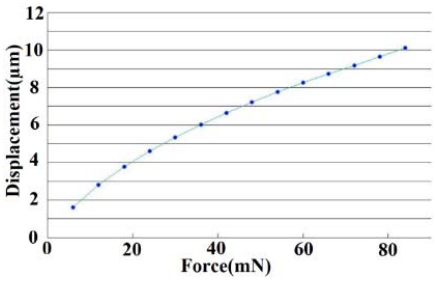

Fig. 10. The force required to deform the *LMA´s* red fork.

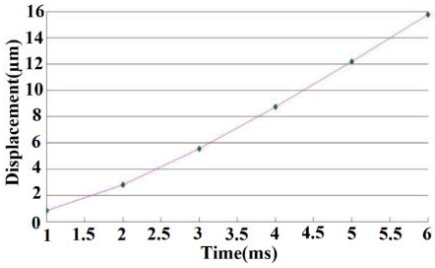

Fig. 11. Deflection of the red fork´s vs. the time.

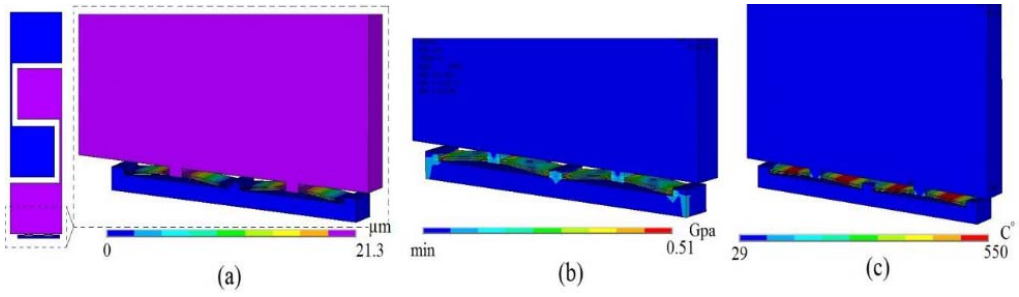

Fig. 12. The contour of the blue and red fork´s deflection (a), the contours of the stress (b), the temperature distribution (c).

5. Conclusion

A favorable propulsion upward or down-ward force can be generated by the LMA, which can cause it to displace heavy loads on the micro and millimeter scales. By repeating sequences, the LMA can reach large travel ranges and has a minimum step size of 20 µm, which is useful for mirror shape correction

applications. The upward or downward propulsion force is approximately 8 mN when using a DC voltage equal to 1.5 volt.

References

[1]. M. J. Daneman, N. C. Tien, O. Solgaard, A. P. Pisano, K. Y. Lau, R. S. Muller, Linear microvibromotor for positioning optical components, *J. Microelectromech. Syst.*, Vol. 5, 1996, pp. 159-165.

[2]. N. R. Tas, T. Sonnenberg, R. Molenaar, M. Elwenspoek, Design, fabrication and testing of laterally driven electrostatic motors employing walking motion and mechanical leverage, *J. Micromech. Microeng.,* Vol. 13, 2003, pp. N6-N15.

[3]. L. Ristic (Ed.), Sensor Technology and Devices, *Artech House*, Norwood, MA, 1994.

[4]. C. S. Pan, W. Hsu, An electro-thermally and laterally driven polysilicon microactuator, *J. Micromech. Microeng*., Vol. 7, 1997, pp. 7-13.

[5]. M. Pai, N. C. Tien, Low voltage electrothermal vibromotor for silicon optical bench applications *Sensors Actuators A*, Vol. 83, 2000, pp. 237-243.

[6]. J. R. Reid, V. M. Bright, J. T. Butler, Automated assembly of flip-up micromirrors, *Sensors Actuators A,* Vol. 66, 1998, pp. 292-298.

[7]. J. S. Park, L. L. Chu, A. D. Oliver, Y. B. Gianchandani, Bent-beam electrothermal actuators: II. Linear and rotary microengines, *J. Microelectromech. Syst*., Vol. 10, 2001, pp. 255-262.

[8]. H. N. Kwon, S. H. Jeong, S. K. Lee, J. H. Lee, Design and characterization of a micromachined inchworm motor with thermoelastic linkage actuators, *Sensors Actuators A*, Vol. 103, 2003, pp. 143-149.

[9]. M. Baltzer, T. Kraus, T. Obermeier, A linear stepping actuator in surface micromachining technology for low voltages and large deflections, in *Proceedings of the IEEE Conference Solid-State Sensors and Actuators*, Chicago, IL, 1997, pp. 781-784.

[10]. Naga Manikanta Kommanaboina, Teferi Sitotaw Yallew, Alvise Bagolini & Maria F. Pantano, A C-shaped hinge for displacement magnification in MEMS rotational structures, nature Journal, Published: 04 January 2024.

[11]. M. P. de Boer, D. L. Luck, W. R. Ashurst, R. Maboudian, A. D. Corwin, J. A. Walraven, J. M. Redmond, A High-performance surfacemicromachined inchworm actuator, *J. Microelectromech. Syst*., Vol. 13, 2004, pp. 63-74.

[12]. T. Risaku, Y. Eui-Hyeok, A normally latched large-stroke, inchworm microactuator, *Micromech. Microeng*., Vol. 17, 2007, pp. 1715-1720.

[13]. J. K. Luo, A. J. Flewitt, S. M. Spearing, N. A. Fleck, W. I. Milne, Modelling of microspring thermal actuator, in *Proceedings of the NSTI-Nanotech Conference*, Vol. 1, 2004, pp. 355-358.

[14]. Z. Yong, C. Alberto, D. E. Horacio, A thermal actuator for nanoscale in situmicroscopy testing: design and characterization, *J. Micromech. Microeng*., Vol. 16, 2006, pp. 242-253.

[15]. B. S. Ang, D. Zuraini, S. Othman, M. Muhamad Azman, Design and analysis of thermal microactuator European, *Journal of Scientific Research*, Vol. 35, Issue 2, 2009, pp. 281-292.

[16]. A. Potekhina, C. Wang, Review of electrothermal actuators and applications school of engineering and physical sciences, *Actuators*, Vol. 8, Issue 4, 2019, 69.

[17]. S. E. Osman, M. Zarog, Optimized V-shaped beam micro-electrothermal actuator using particle swarm optimization (PSO) technique, *Micro and Nanosystems*, Vol. 11, Issue 1, 2019, pp. 62-67.

[18]. M. Chiao, L. Lin, Self-buckling of micromachined beams under resistive heating, *J. Microelectromech. Syst.,* Vol. 9, 2000, pp. 146-151.

[19]. O. Ulkir, Design and fabrication of an electrothermal MEMS micro-actuator with 3D printing technology, *Materials Research Express*, Vol. 7, Issue 7, 2020, 075015.

[20]. P. D. Pour, Dr. M. Ghommem, Dr. A. Abdelkefi, Modeling and design enhancement of electrothermal actuators for microgripping applications, *Appl. Sci*., Vol. 13, Issue 18, 2023, 10140.

[21]. D. Hill, W. Szyszkowski, E. Bordatchev, On modeling and computer simulation of an electro-thermally driven cascaded nickel microactuator, *Sensors and Actuators A*, Vol. 126, 2006, pp. 253-263.

[22]. I. H. Hwang, J. H. Lee, Novel measurement system of the friction coefficients for the DRIE sidewalls, in *Proceedings of the IEEE International Conference on Micro Electro Mechanical Systems*, 2006, pp. 210-213.

[23]. S. Ramya, S. Praveen Kumar, T. Aravind, U. Rasan, G. Dinesh Ram, D. Lingaraja, Design of chevron electrothermal actuator for high force defense applications, in *Proceedings of the 7th International Conference on Computing Methodologies and Communication (ICCMC'23)*, 2023, pp. 1-3.

[24]. S. Memon, S. Khan Baloch, S. Rehman Soomro, I. Ali Tunio, O. Ur Rehman, S. Ahmed, Design and finite element modeling of electro-thermal actuator for biological applications, *Journal of Computing & Biomedical Informatics*, Vol. 5, Issue 1, 2023.

[25]. H. Xie, H. Yang, A. R. Y. Ding, L. Xiao,T. Pan, Y. Yan, W. Jiao, A robust lateral shift free (LSF) electrothermal micromirror with flexible multi-morph beams, *Microsystems & Nanoengineering*, Vol. 9, 2023, pp.1-12.